Science of the Total Environment 912 (2024) 169280

Contents lists available at ScienceDirect

Science of the Total Environment

journal homepage: www.elsevier.com/locate/scitotenv

Microplastic retention in marine vegetation canopies under breaking irregular waves

Nils B. Kerpen [a], Bjarke Eltard Larsen [b], Torsten Schlurmann [a], Maike Paul [a], Hasan Gokhan Guler [b,c], Koray Deniz Goral [b], Stefan Carstensen [b], Erik Damgaard Christensen [b], David R. Fuhrman [b,*]

[a] Gottfried Wilhelm Leibniz University Hannover, Ludwig-Franzius-Institute for Hydraulic, Estuarine and Coastal Engineering, Nienburger Str. 4, D-30167 Hannover, Germany
[b] Technical University of Denmark, Department of Civil and Mechanical Engineering, DK-2800 Kgs. Lyngby, Denmark
[c] Middle East Technical University, Department of Civil Engineering, Ocean Engineering Research Center, Cankaya, Ankara, Turkey

HIGHLIGHTS

- Microplastic retention in marine canopies for irregular waves over a sand bed.
- Fringe regions are proven to be a barrier and sink for microplastics.
- Retention varied by particle Dean number and increased with shoot density.
- A mathematical scheme is derived to approximate the particle retention potential.

GRAPHICAL ABSTRACT

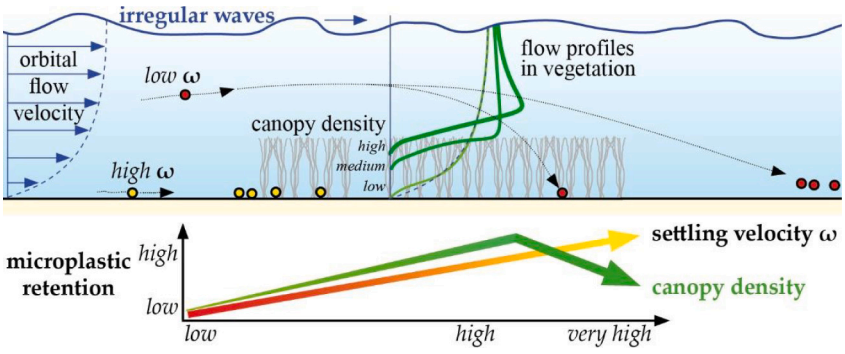

ARTICLE INFO

Editor: Damià Barceló

Keywords:
Particle transport
Particle retention
Submerged canopy
Canopy density
Canopy flow
Particle Dean number

ABSTRACT

The present study provides indications and underlying drivers of wave-induced transport and retention potential of microplastic particles (MP) in marine vegetation canopies having different densities. The anthropogenic occurrence of MP in coastal waters is well documented in the recent literature. It is acknowledged that coastal vegetation can serve as a sink for MP due to its energy dissipating features, which can mimic a novel ecosystem service. While the transport behavior of MP in vegetation has previously been investigated to some extent for stationary flow conditions, fundamental investigations for unsteady surf zone flow conditions under irregular waves are still lacking. Herein, we demonstrate by means of hydraulic model tests that a vegetation's retention potential of MP in waves increases with the vegetation shoot density, the MP settling velocity and decreasing wave energy. It is found that particles migrating by traction (predominantly in contact with the bed) are trapped in the wake regions around a canopy, whereas suspended particles are able to pass vegetated areas more easily. Very dense canopies can also promote the passage of MP with diameters larger than the plant spacing, as the canopies then show characteristics of a solid sill and avoid particle penetration. The particle migration ability through a marine vegetation canopy is quantified, and the key drivers are described by an empirical expression

* Corresponding author.
E-mail address: drfu@dtu.dk (D.R. Fuhrman).

https://doi.org/10.1016/j.scitotenv.2023.169280
Received 12 May 2023; Received in revised form 7 December 2023; Accepted 9 December 2023
Available online 19 December 2023
0048-9697/© 2023 The Authors. Published by Elsevier B.V. This is an open access article under the CC BY license (http://creativecommons.org/licenses/by/4.0/).

based on the particle settling velocity, the canopy length and density. The findings of this study may contribute to improved prediction and assessment of MP accumulation hotspots in vegetated coastal areas and, thus, may help in tracing MP sinks. Such knowledge can be considered a prerequisite to develope methods or new technologies to recover plastic pollutants and rehabilitate valuable coastal environments.

1. Introduction

Millions of tons of plastic enter the world's oceans every year (van Sebille et al., 2020b). It has been estimated that the cumulative amounts have increased by an order of magnitude over the past decade, with a further 50-fold increase expected by year 2100 (Everaert et al., 2018). Of particular concern are particles in the microplastic regime, having length scales <5 mm (Galgani et al., 2013). The fate of microplastic in the ocean involves complex interactions, including fragmentation (Song et al., 2017; Gerritse et al., 2020), transport (Zhang, 2017; van Sebille et al., 2020b), ingestion by marine organisms (Deudero and Alomar, 2015), and potential accumulation in sediments (Wessel et al., 2016; Harris, 2020), posing environmental concerns and potential threats to marine ecosystems (Cózar et al., 2015). Aquatic coastal environments such as dune ecosystems, salt marshes, seagrass meadows or mangrove forests provide important ecosystem services (e.g. water quality improvement, habitat creation, or carbon sequestration) and benefits (e.g. flood control, biodiversity support or shoreline stabilization) (Duarte et al., 2013). The trapping of microplastic particles (MP) and sediments by coastal plant communities, due to the alteration of near-bed hydrodynamics and transport processes, have been reported in numerous publications (Huang et al., 2020; de Smit et al., 2021; Duan et al., 2021; Sanchez-Vidal et al., 2021; Contti Neto et al., 2022; Li et al., 2022; Maghsodian et al., 2022; Ogbuagu et al., 2022; da Silva Paes et al., 2022; Battisti et al., 2023; Ben-Haddad et al., 2023). In addition to these field observations, the trapping and retention potential of vegetation have been documented in laboratory studies under steady flow conditions (de los Santos et al., 2021; Gallitelli et al., 2023). Research on the trajectory and distribution of MP in complex coastal environments, especially quantitative, is needed (Duan et al., 2021).

Framing of the present study, in relation to the existing literature addressing key drivers of MP transportation processes in the coastal environment, is provided in a background section through a brief overview on wave hydrodynamics on the bottom boundary layer in the surf zone, their influence on MP transport with respect to the MP properties and the energy damping characteristics of vegetation patches. Hereafter, Materials and Methods are introduced. The results and discussion section examines wave characteristics and beach profile evolution, flow conditions within submerged vegetation canopies, the cross-shore distribution of microplastic particles in these canopies, the ability of particles to migrate cross-shore, and a detailed description of observed transport mechanisms. Finally, the findings of the study are summarized and implications are drawn in the conclusions.

2. Background

This chapter briefly introduces to (i) flow-conditions in the surf-zone induced by waves and currents, (ii) the influence of these flows on MPs, by means of the particle Dean number and (iii) the energy dissipation in submerged vegetation patches.

2.1. Surf-zone hydrodynamics

In the coastal zone particles are exposed to forces induced by currents, wave-induced oscillations and turbulence induced by wave breaking or fluid-seabed interaction (Dean and Dalrymple, 1991). These active forces govern the transport, sedimentation and re-suspension of MP. The forces (and thereby the transport) are naturally dependent on the water level and wave conditions. Baltic amber (with a density similar to plastic), for instance, migrates towards the shore during storms (Chubarenko et al., 2018). Wave-induced hydrodynamics in the surf zone represent an extremely turbulent and complex regime, which has previously been investigated in small scale model tests (Ting and Kirby, 1994) and large-scale model tests with respect to flow and sediment transport processes (Scott et al., 2005; Cáceres and Alsina, 2012; Van der Zanden et al., 2016, 2017). In the present study, we replicate the evolution of a beach profile by drawing upon prior research on MP transport in irregular waves (Guler et al., 2022; Larsen et al., 2023b), effectively establishing consistent hydraulic boundary conditions. This approach allows us to determine the influence of vegetation, relative to the previously determined MP transport processes without vegetation. The underlying hydrodynamic transport processes in this configuration are described in more detail by Larsen et al. (2023b). A comparison between the present study and these references on the beach profile evolution over time and the corresponding energy decay is provided in Kerpen et al. (2023).

2.2. MP properties and transport ability

While fluid-driven sediment transport mechanisms have been studied for decades (Inman, 1949; Yalin, 1977; Van Rijn, 1993; Soulsby, 1997; Nielsen, 2009), hydraulic model experiments on non-buoyant MP transport are rare. Size, shape and density of MP have a significant influence on their transport properties (Ballent et al., 2013; Zhang, 2017; Waldschläger and Schüttrumpf, 2019; van Sebille et al., 2020a; Goral et al., 2023). MP transport in steady currents has been considered in several studies (de los Santos et al., 2021; Valero et al., 2022; Gallitelli et al., 2023; Núñez et al., 2023). However, wave-driven surf zone flows have different flow mechanisms and thus, e.g. MP transport processes and rates will differ. To date, the wave-driven transport of non-buoyant MP in shallow coastal waters has been studied by few authors. The accumulation of heavy MP in the wave breaking (surf) zone, as well as accumulation of light MP along the coastal profile, was previously investigated in idealized short duration model tests over a fixed beach profile with constant slope (Forsberg et al., 2020). Long duration experiments on MP transport with regular waves on a live sediment bed revealed a shift of the accumulation peak of typical MP fractions into shallower water depths, with increasing particle size and density (Kerpen et al., 2020). Considering the importance of the MP settling velocity on the location of MP accumulation (Kerpen et al., 2020), the transport of non-buoyant MP beneath breaking irregular waves on a live sediment bed is primarily governed by the dimensionless particle Dean number (Guler et al., 2022; Núñez et al., 2023):

$$\Omega_p = \frac{H_0}{T_p \omega_{sp}} \tag{1}$$

which relates the characteristic deep water wave height H_0 to the peak wave period T_p and the MP settling velocity ω_{sp}. The particle Dean number can be interpreted as a dimensionless descent rate. Furthermore, the nearshore transport of buoyant MP across a coastal profile can be predicted based on the wave-induced transport velocity (Larsen et al., 2023a). In these five studies, vegetation was not taken into account. A relation to the particle Dean number may likewise be relevant for transport in vegetation patches, but such knowledge is presently lacking. Hence, the present study will address the results of these previous studies and examine the influence of vegetation on the resulting migration pathways of MP.

2.3. Energy dissipation by submerged vegetation patches

It is known that stiffness, shoot density and submergence ratio are decisive factors for the reduction of flow velocities and wave heights (Pujol et al., 2013; Jacobsen and McFall, 2022) in vegetated areas. This has also been shown in field studies for seagrass meadows (Bradley and Houser, 2009; Paul and Amos, 2011). A wake region with reduced velocities behind vegetation stands can form (Villanueva et al., 2022), which can promote sediment settling and reduce resuspension. The latter was observed for a *Ruppia maritima* dominated meadow where Suspended Particulate Material (SPM) was not affected by a high wind event, whereas SPM concentrations increased in an adjacent unvegetated area during this event (Ward et al., 1984). Given the close link between wave or flow induced shear velocities and sediment resuspension (Lawson et al., 2007), SPM concentrations in seagrass meadows equally depend on shoot density (Newell and Koch, 2004) and submergence ratio (Ward et al., 1984). More recent measurements of velocity and suspended sediment concentrations within and above a mixed seagrass meadow have shown that the boundary layer which develops at the top of a seagrass canopy leads to the independence of SPM concentrations within the canopy from hydrodynamic conditions above (Contti Neto et al., 2022). Processes of enhanced sediment settling, on the other hand, have not yet been directly measured in natural seagrass meadows. However, it has been inferred from grain size distributions (van Katwijk et al., 2010) or bathymetry (Eklöf et al., 2015) and is a widely accepted ecosystem service of seagrass meadows globally (Nordlund et al., 2016). It is hypothesised that the governing processes can lead to trapping of MP in vegetated areas, and Sanchez-Vidal et al. (2021) found that MP can indeed become trapped in the filamentous debris of *Posidonia oceanica*. However, the MP transport pathways inside seagrass meadows under irregular waves have yet to be investigated, either in the field or in indoor (laboratory) conditions. The present paper will analyse the influence of vegetation patches on the migration of MP and provide a mathematical scheme for predicting particle retention. The paper seeks to elucidate the mechanism by which vegetation entraps particles that would have otherwise passed through an unvegetated area. The paper does not aim to quantify how many particles will be trapped within a vegetation.

Having introduced important aspects of surf-zone hydrodynamics, the properties and transport ability of MP, and the energy dissipation by submerged vegetation patches, Section 3 will outline the present experimental set-up and procedure, the characteristics of MP and vegetation to be considered, and concludes with some analytical considerations. The migration and retention of six different MP groups with varying particle Dean numbers ($0.36 \leq \Omega_p \leq 1.62$) under (predominantly breaking) irregular waves are studied. The canopy is simulated with four different canopy densities (defined in forthcoming Eq. 2 and ranging from $\phi = 0.007$ to 1.59).

3. Materials and methods

3.1. Wave flume and instrumentation

To investigate the influence of submerged vegetation on the wave-induced migration of MP, physical model tests were carried out in a wave flume at Ludwig-Franzius-Institute, Leibniz University Hannover. The flume is 6.5 m long, 0.3 m wide and 0.45 m deep. Second-order irregular waves were generated by a piston wave maker. The side view of the experimental set-up is presented in Fig. 1a, with the origin placed at the intersection of the wave maker ($x = 0$) and the bottom of the beach plateau, and with the vertical z-axis pointing upwards.

Wave characteristics were recorded along the beach slope by ultrasonic wave gauges (WG 1–6, brand: USS10 by General Acoustics e.K., sampling frequency: $f_s = 100$ Hz, vertical resolution: $\delta_z = 0.2$ mm, position: $x = \{0.05, 1.09, 1.77, 2.34, 2.93, 3.58\}$ m). In order to describe the influence of the vegetated area on the MP transport, knowledge of local flow intensities is important. A flow profile ($0 \leq z \leq 30$ mm, $\delta_z =$ 1 mm vertical resolution) was measured with a Nortek Acoustic-Doppler Velocimeter (Vectrino Profiler, ADV, sampling frequency: $f_s = 50$ Hz) located above the vegetation canopy ($x = 2.7$ m, $y = 0.15$ m, Fig. 1b). Velocities were calculated from the raw data by applying a signal-to-noise threshold-value of >15 dB and a signal correlation of >90 %. MP were released 0.1 m (5 times the vegetation height h_v) off- and onshore the implemented canopies. The average of the measured water

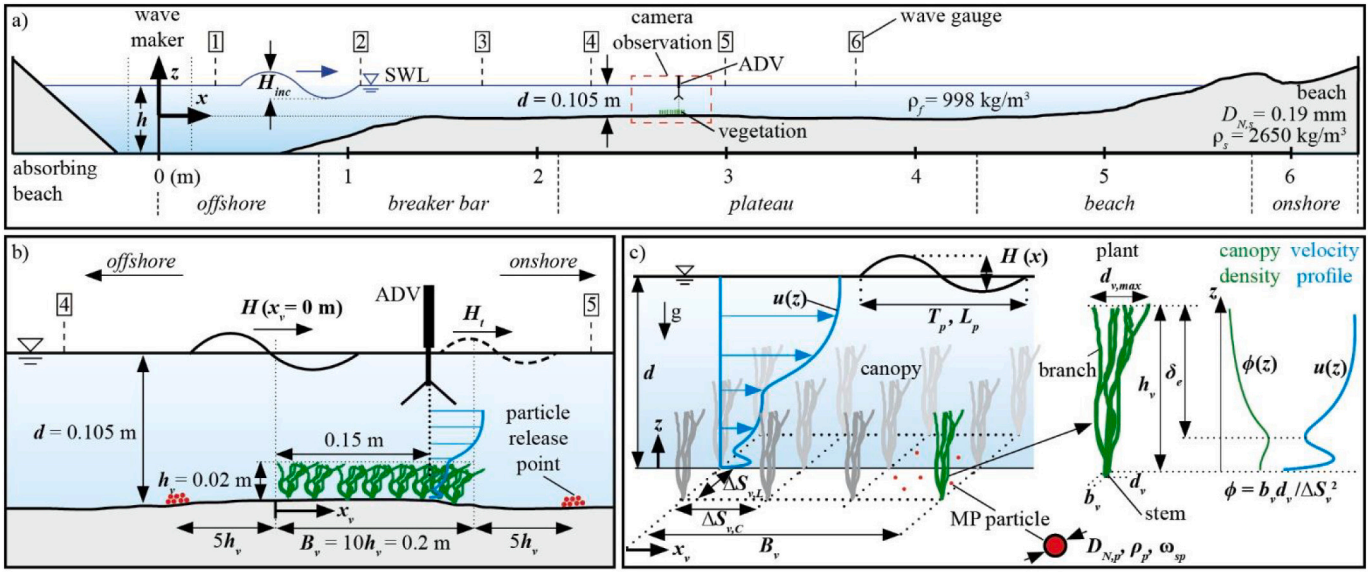

Fig. 1. a) Side view of the model set-up in the wave flume with dynamic beach profile (developed from an initial 1:25 slope after 170 h of wave exposure), vegetation canopy location, location of instrumentation (six wave gauges [1]–[6], one ADV, camera observation frame). Definition of beach profile areas are provided. b) Detail (dashed red square in subfigure a)) of the vegetated investigation area in the wave flume ($x_v = 0$ m at $x = 2.55$ m) with MP (red) release points at the beginning of each experiment. The position of the ADV with indicated flow profile (blue) close to the vegetation canopy. c) Parameters defined for the submerged canopy and a single plant including qualitative profiles along the z-axis for the canopy density and the velocity profile. The canopy density profile $\phi(z)$ and the velocity profile $u(z)$ in the canopy are inspired by Nepf (2012) for steady currents.

temperatures throughout the experiments was 19.8 °C, the corresponding density of the water was determined to be $\rho_f = 998\,\mathrm{kg/m^3}$, and the corresponding kinematic viscosity to be $\nu = 1.01 \times 10^{-6}\,\mathrm{m^2/s}$. The principal characteristics of a submerged canopy can be described by the parameters defined in Fig. 1c. Further details about the parameters defining the vegetation and canopy properties will be provided in Section 3.3.

3.2. Microplastic particles

MP have been selected to show clear on- or offshore migration directions in the plateau region in a case without vegetation. The corresponding particle migration direction is mostly governed by the particle Dean number (Guler et al., 2022). The six analyzed particle groups (50 particles each) and their properties are listed in Kerpen et al. (2023). All examined particles had an irregular shape, but may be considered as reasonably spherical (settling sphericity: $0.84 < \psi = \left(c^2/(ab)\right)^{1/3} \leq 1.0$ with a, b, c as the particles *xyz*-dimensions respectively). The transport mode of a particle is mainly influenced by the ratio of the acting local flow velocity u to the particle settling velocity ω_{sp}. The settling velocity of a particle depends on the geometric particle shape and the difference in density relative to the surrounding viscous fluid (Dietrich, 1982). An increasing particle drag force causes a decreasing particle settling velocity. The mode of transportation (bedload or suspended load) of an MP is directly related to the ratio of u/ω_{sp}. During the tests involving breaking wave-induced flow over the sediment bed, suspension of MP having the highest tested particle Dean numbers $\Omega_p = 1.6$ (with a corresponding low particle settling velocity) has been observed for a number of waves. Close observation has revealed that this suspension occurred in conjunction with bed ripples. Particles with Dean number $\Omega_p = 1.08$ were transported mainly as bed load, rolling, sliding, and saltating (jumping) over the bed. In the Dean number regime $0.58 < \Omega_p < 0.66$ most particles demonstrate a saltating transport, getting momentarily lifted from the bed by accelerated flows and pulled immediately downwards by gravity. Particles in the lowest tested Dean number regime ($\Omega_p = 0.36$) were in continuous contact with the bed and were transported through traction (rolling). A graphical representation of the different transport features of MP is given in the discussion at the end of the present paper (see forthcoming Fig. 7).

In relation to the tested near-bed flow velocity amplitude stemming from the selected hydraulic boundary conditions (Section 3.4) the MP diameters were comparatively large. This selection was made for two reasons: First, to be able to clearly visualize, trace and identify the particles in the test area; Second, to enable a direct comparison of findings from the present study with the prior experiments conducted by Guler et al. (2022), who have studied non-buoyant microplastic transport beneath breaking irregular waves on a live sediment bed without the presence of vegetation. We tested similar hydraulic and geometric boundary conditions in order to address the influence of vegetation to the principle findings from Guler et al. (2022). Findings stemming from the present study can be reasonably transferred to larger scales or even to natural environments, provided that the most important non-dimensional numbers are similar. These critical parameters include the Dean number of the plastic and sand, the canopy density, the wave steepness and the relative submergence of vegetation. For more detailed dimensional analysis without vegetation see Guler et al. (2022).

3.3. Vegetation

The characteristics of a submerged canopy are described by a number of parameters defined in Fig. 1c. In principle, a canopy consists of a number of individual plants. The shoot density defines the number of plants per square meter. The height of the plant and the canopy is defined as h_v. A plant is composed of a stem (length: $b_{v.}$, width: $d_{v.}$) and a number of branches sprouting from it. The fanning width of the branches is denoted $d_{v,max}$. The spacing between the individual plants in the canopy is defined in both long-shore ($\Delta S_{v,L}$) and cross-shore ($\Delta S_{v,C}$) directions. With these parameters, the canopy density

$$\phi = \frac{b_v d_v}{\Delta S_{v,L} \Delta S_{v,C}} \tag{2}$$

represents the solid volume fraction, and is defined according to Nepf (2012). As the diameters of the branches decrease with increasing elevation ($z > 0$), the canopy density also decreases. The bottom flow velocity u reduces with increasing canopy density as the cross-sectional area flowed through is reduced. The canopy shear layer depth δ_e defines the penetration depth of the canopy-scale turbulence (Nepf, 2012) from the top of the canopy towards the bottom, which causes a local minimum in the velocity profile.

The vegetation in the present tests considered four different densities, where the very sparse density was mimicked by a 3D printed pile-group arrangement, and the other three stemmed from artificial turf mats. The variation of the canopy density was conducted by removing individual plants from a pre-fabricated mat with a very homogeneous, yet seemingly artificial pattern, e.g. homogeneous rows with machine fabricated structure. At first, the original turf mat (dense canopy layout) was tested. The transitional layout was manufactured by removing individual plant bundles in a checkerboard pattern from the original turf mat. To receive the sparse canopy density each 2nd row (in the long-shore direction) from the former transitional layout was manually removed. The specifications of the four tested vegetation canopies and an image of the three artificial turf mats are given in Kerpen et al. (2023). The shoot densities were selected to create canopy densities corresponding to a sparse ($\phi \ll 0.1$), a transitional ($\phi \simeq 0.1$) and a dense ($\phi > 0.1$) canopy, following the definitions of Nepf (2012). The modification of the long-shore spacing $\Delta S_{v,L}$ between two plants (orthogonal to the flow direction) shows a much greater influence on the flow resistance of the canopy than the cross-shore spacing (Gijón Mancheño et al., 2021). The tested dense and transitional canopies differed in the long- and cross-shore spacing of plants. The transitional and sparse canopies differed in the long-shore spacing of plants. Consequently, the dense and sparse canopies differed in cross- and long-shore spacing of individual plants.

The local water depth was constant ($d = 0.105\,\mathrm{m} \pm 5\,\%$) throughout the tests and mimicked a prototype depth of 2.1 m in a scale of 1:20, since many species build marine habitats in water depth of 1 to 3 m (Krause-Jensen et al., 2000; Dolch et al., 2013; Schubert et al., 2015). The investigated canopy height of $h_v = 2\,\mathrm{cm}$, in combination with the selected scaling, likewise represents realistic environmental conditions for seagrass meadows with heights of 40 cm (de los Santos et al., 2016; Paul and de los Santos, 2019). All canopies were tested in a shallow submergence regime ($d/h_v \leq 5$), which is common in aquatic systems (Nepf and Vivoni, 2000). In this regime canopy-scale vortices – Kelvin-Helmholtz vortices triggered by flow instabilities at the top interface of transitional and dense canopies – dominate the turbulence field within and above the canopy (Ghisalberti and Nepf, 2008). The present experiments represent this complex flow process, which influences the transport, penetration and re-suspension, and therefore the cross-shore distribution, of MP.

3.4. Experimental procedure

The geometric and hydraulic boundary conditions have been selected to mimic the experimental conditions of Guler et al. (2022) at a scale of 1:2.5, since the wave-driven transport of a wide variety of MP without vegetation has previously been studied in detail in this series of experiments. The hydraulic parameters are representative boundary conditions of the North Sea (mean wave height of 1.04 m and peak periods in the range of 3–6 s, recorded off the coast of the Island of Sylt, Germany, at the station “Westerland” in 2021 by BSH (2021)) at a model

scale (Froude scaling) of about 1:20. The beach profile in the present set-up was developed from an initially plain beach slope of 1:25. The sand used to construct the bottom configuration had a median diameter of $D_{N,s} = 0.19$ mm and a density of $\rho_s = 2650\ \mathrm{kg/m^3}$. The irregular wave conditions and the toe water depth in front of the wave maker ($h = 0.2$ m) remained constant throughout all tests. The wave characteristics followed a JONSWAP spectrum (Hasselmann, 1973) with peak enhancement factor of $\gamma = 3.3$, spectral significant wave height $H_{m0} = 0.06$ m and peak period $T_p = 1.0$ s (peak wave length $L_p = 1.2$ m, peak wave number $k_p = 2\pi/L_p = 5.2\ \mathrm{m^{-1}}$, dimensionless characteristic depth $k_p h = 1.1$ and wave steepness $H_{inc}/L_p = 0.05$) and a length of the time series of 10 min (about 650 individual waves). This time series was continuously repeated for the duration of each test. A long test duration with a high number of waves (Table 1) was selected in order to achieve a kind of dynamic profile equilibrium for the retention of the individual particles in the system. Note that Larsen et al. (2023b) and Guler et al. (2022) have formerly confirmed that this profile shape is indeed close to equilibrium. The barred beach profile presented in Fig. 1 resulted from wave-induced morphodynamic processes after >680,000 irregular waves (170 h test time). The evolution of the beach profile and measured wave heights along the flume are provided in comparison with the tests from Guler et al. (2022) in Kerpen et al. (2023). Consistent with expectations from above, the final beach profile ($t = 170$ h) represented a quasi-equilibrium state, which did not change significantly during further investigations involving the interaction of MP with vegetation (consecutive 10 h test duration each run).

As stated above, the water level in the vegetated area ($d = 0.105$ m) remained nearly constant during the tests (±5 % variation as a result of the dynamic sand bed). At the beginning of each test, the initial bed profile depth d in the observation region was restored. A reference test had been performed in the barred profile configuration (Test nr. 101). Six groups of MP with varying particle characteristics (50 particles each, (Kerpen et al., 2023) were released over the barred beach profile at $x = 2.6$ m. After 10 h of irregular wave loading (>40,000 waves) the cross-shore distribution of the MP groups was documented in order to identify how the particles were transported and where they accumulated without vegetation. Subsequently, four vegetation canopies with varying canopy density ($0.007 < \phi < 0.159$) were placed above the barred sediment bed over a length of $B_v = 0.2$ m ($B_v/h_v = 10$, $B_v/L_p = 0.125$) in sequences (Test nr.102 to 105). Based on the observations from the reference test, particles that migrated offshore (particle 'L') were placed on the on-shore side of the canopy ($x = 2.85$ m), and the MP groups that migrated onshore on the offshore side ($x = 2.45$ m). This approach was selected in order to force the particles to migrate through the installed canopy. After each test, a manual spatial allocation and counting of the individual MP was conducted. The state of the beach profile was documented by a camera (single side view images of the flume section given in Fig. 1a) before and after each test run, camera: Canon EOS 2000D, image resolution: 6000x4000 px). Finally, Test nr. 101 without vegetation was repeated one more time (Test nr. 106) after all tests with vegetation, in order to prove the repeatability of findings and demonstrate that wave and flow conditions were effectively constant throughout all tests.

4. Results and discussion

4.1. Wave energy dissipation and beach profile evolution

The wave characteristics along the beach profile throughout the tests, as well as the beach profile evolution itself, will be briefly outlined. Corresponding data are provided in Kerpen et al. (2023). In all experiments, the wave height decreased along the flume due to increasing energy dissipation induced by bottom friction and depth limited wave breaking with decreasing water depth and increasing propagation distance from intermediate water depth ($k_p h = 1.05$) towards the beach ($H_{WG6(x=3.58\mathrm{m})} = 0.69 H_{WG1(x=0.05\mathrm{m})}$, (Kerpen et al., 2023)). Due to the relatively short cross-shore dimension of the investigated canopies ($B_v/L_p = 0.125$) and emergent canopy conditions ($d/h_v = 5$), the influence of the vegetation on the energy dissipation of the waves in these experiments was approximately 2 %, and so almost negligible (e.g. Test nr. 103: $H_{WG6(x=3.58\mathrm{m})} = 0.67 H_{WG1(x=0.05\mathrm{m})}$). Nevertheless, the near-bed hydrodynamics were altered by the presence of the vegetation, and these will therefore be analyzed in greater detail in what follows.

4.2. Flow conditions in the canopy environment

Knowledge about local flow intensities enables characterization of the MP transport processes in vegetation canopies. Fig. 2 provides absolute values of measured flow velocities over the canopies for different canopy densities $0 \le \phi \le 0.159$. RMS flow profiles are provided for onshore (blue solid line) and offshore (red solid line) directed flows (based on a wave period's half cycle). For the onshore direction corresponding lower 25 % and upper 75 % quantiles of the averaged flow velocities are provided with box-plots.

Without vegetation ($\phi = 0$, Fig. 2a), the flow velocity profile shows a fairly constant amplitude, slightly decreasing towards the bottom due to bed shear forces. For comparison, the RMS horizontal velocity profile $\widetilde{u}_{+x}(z)$ is provided (Fig. 2a, black dashed line) according to the estimated medium orbital velocity component in the positive x-direction from Eq. (A.3) (again, based on a wave period's half cycle).

For very sparse vegetation ($\phi = 0.007$, Fig. 2b) the flow profile clearly indicates influence of the vegetation on the near-bed flow. Disproportionate gradients within the flow profile (e.g. at interface of the vegetation and the free flow region) indicate increased turbulence caused by vortex shedding. This effect is similarly described by Raupach et al. (1996). Additionally, a reduction in the flow amplitude towards the bottom is measured at $z < 0.25 h_v = 0.005$ m.

With increasing vegetation canopy density ($\phi = 0.028$, Fig. 2c) a canopy shear layer evolves with a distance of δ_e from the canopy top. Below this level, the measured flow velocity is almost zero. Close to the top of the canopy the flow amplitudes increase slightly. Above the canopy, the offshore directed flow amplitude (red line) is nearly constant, whereas the onshore directed flow amplitudes (blue line) show a decay with distance to the canopy. This difference might be explained by the different distances to the edges of the canopy from the measurement point (0.15 m to the offshore edge influencing the onshore oriented velocities and 0.05 m to the onshore edge influencing the offshore oriented velocities; compare with Fig. 1b). The processes just described

Table 1
Description of the experimental runs. The total number of particles of each type was $N = 50$ in each experimental run.

Test nr.	Initial bed configuration	Canopy density ϕ	Test duration (t_{end}, hr)	Number of waves	Particles used (no. buried in parentheses)
001–055	Plain (1:25)	0	170	688,620	–
101	Barred profile	0	10	40,956	A (1), B (1), G(0), H(1), L (3), N (0)
102	Barred profile	0.007	10	40,498	A (9), B (3), G(0), H(1), L (0), N (0)
103	Barred profile	0.159	10	40,496	A (2), B (2), G(0), H(0), L (0), N (0)
104	Barred profile	0.058	10	40,671	A (0), B (1), G(0), H(0), L (0), N (0)
105	Barred profile	0.028	10	41,078	A (0), B (1), G(0), H(0), L (0), N (0)
106	Barred profile	0	10	41,342	A (1), B (2), G(0), H(1), L (4), N (0)

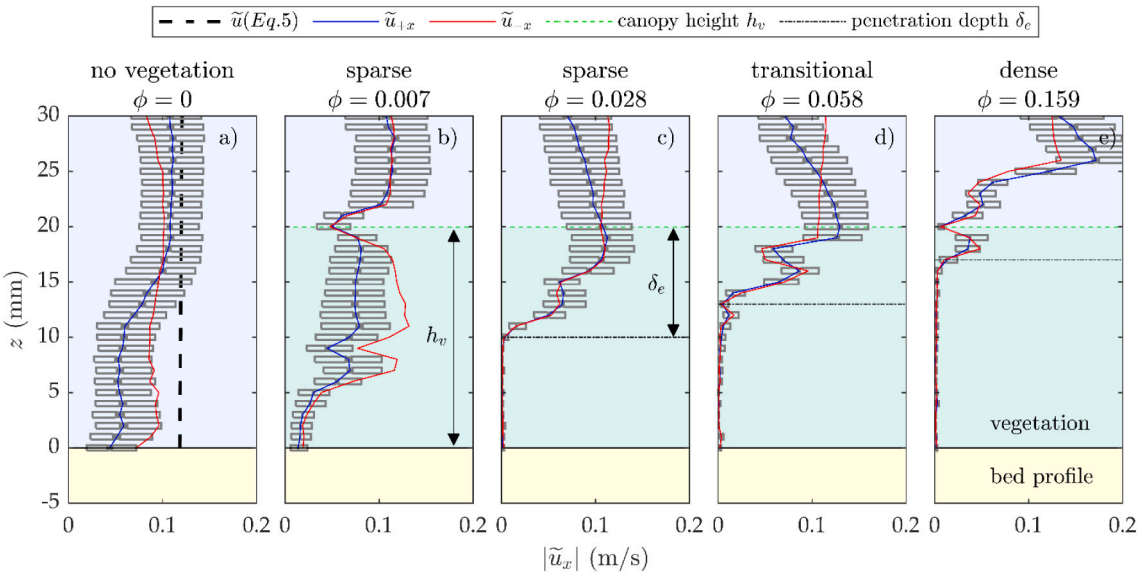

Fig. 2. Flow profiles (at $x = 2.7$ m, respectively $x_v = 0.15$ m) from RMS flow velocities in x-direction $\widetilde{u}_x(z)$ for varying canopy densities ($0 \leq \phi \leq 0.159$). Onshore directed ($\widetilde{u}_{+x}$): blue solid line with corresponding lower 25 % and upper 75 % quantiles. Offshore directed ($\widetilde{u}_{-x}$): red solid line without quantiles. Canopy heights h_v are highlighted by a green dotted line and the canopy shear layer depth δ_e by a black dashed-dotted line.

amplify with increasing canopy density ($\phi = 0.058$, Fig. 2d).

For the dense canopy configuration ($\phi = 0.159$, Fig. 2e), almost no penetration of the flow into the canopy was measured. Instead, a strongly flow-calmed shear area is measured up to 5 mm above the canopy. Above this area, a clearly increased flow amplitude is measured.

Fig. 3 depicts the previously described influence of the various canopies on the measured RMS flow velocity $\widetilde{u}_x$ relative to that without vegetation $\widetilde{u}_{\phi=0}$. The depth in the canopy is given for the normalized water depth $z^* = (z + d)/h_v$ with the top of the canopy at $z^* = 1$. In these terms, it becomes apparent that very sparse vegetation ($\phi = 0.007$) leads to turbulent fluctuations along the flow profile but no significant influence on the RMS flow profile compared to no vegetation ($\widetilde{u}_x/\widetilde{u}_{\phi=0} \approx 1$). With increasing canopy density the flow amplitude in the deeper canopy regions tends towards zero, whereas the flow amplitudes

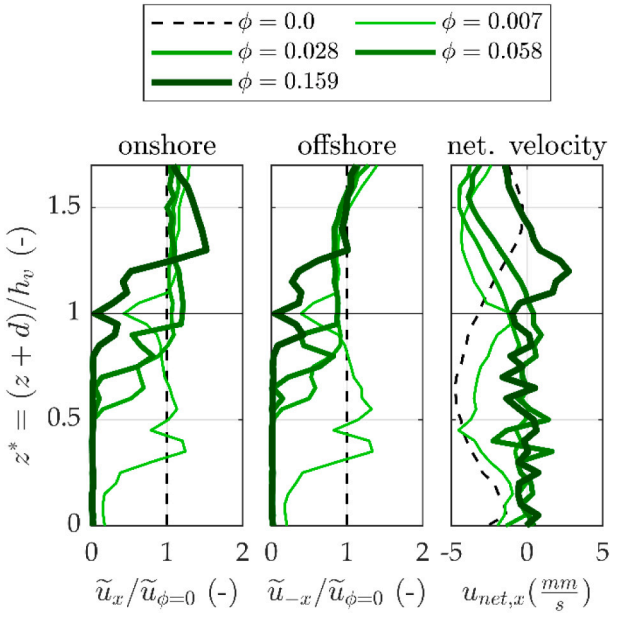

Fig. 3. Onshore, offshore profiles normalized by the RMS flow velocity without canopy ($\widetilde{u}_{\phi=0}$) and net velocity with respect to the normalized water depth z^*.

above the canopies tend to increase. The highest canopy density leads to the clear formation of a shear layer with reduced RMS flow velocities above the canopy and above that the highest flow velocities compared to a situation without the presence of vegetation. For rigid canopies, this layer of amplified flow velocities above the top of the vegetation canopy, and a layer of reduced flow velocities directly below the top of the vegetation canopy; was previously documented for unsteady currents (Van Veelen et al., 2020). The net velocity profile without vegetation clearly indicates the presence of an offshore directed undertow. This flow is marginally affected by the very sparse vegetation. The provided amplitude might be overestimated since the velocity probe is not located in the center of the meadow (Fig. 1b) and the offshore directed flow passes only 1/3 of the canopy distance compared to the onshore directed flow. With increasing canopy density, the net flow velocity inside the canopy tends towards zero. For the densest canopy, an onshore directed net velocity directly above the canopy evolves.

The current investigation reveals that the mean positive and negative amplitude of the flow in a depth of $z^* = 0.3$ has almost the same value as an unvegetated area (Fig. 3). This observation is confirmed by velocity measurements in a seagrass meadow at Garden Island, Western Australia, with boundary conditions comparable to those presented in the present study ($d/h_v = 4.29; \sim 400$ shoots/m^2) (Contti Neto et al., 2022). They found that near-bed ($z^* \sim 0.3h_v$) mean current velocities within a seagrass canopy were reduced to an average of 35 % relative to those above the canopy, and for surf zone flow velocities, less attenuation (83 % of those above the canopy). Therefore, the relatively low wave energy dissipation for sparse canopies is replicated in the present tests. On the other hand, it is known that wave attenuation is up to 70 % less in flexible vegetation, relative to rigid vegetation (Van Veelen et al., 2020). A comparison with this value is not possible with the data from the present study, as (1) the tested canopy width is relatively short ($B_v/L = 0.125$) and (2) the tests with rigid (Test no. 102) and flexible (Test no. 103–105) vegetation have different canopy densities. Nevertheless, due to scale effects, the energy dissipation for the artificial grass meadows in the present study might be over-estimated relative to natural conditions as the stiffness may be too large during an upscaling.

The measured flow amplitudes in deeper regions of the tested canopies might be biased, as the acoustic measuring principle of the ADV sensor might be affected by the presence of vegetation. The measurement of dense canopy dynamics well below the threshold defined in

Nepf (2012) might indicate this limitation. Even though this impact cannot be ruled out, it is expected to be minor, especially given the general agreement with flow profiles from other studies (Defina and Bixio, 2005; Nepf et al., 2007).

4.3. Cross-shore distribution of MP

The cross-shore distributions of the MP at the end of each test run are provided in Fig. 4, separated by vegetation density (columns, with ascending ϕ) and particle Dean numbers (rows, with ascending Ω_p). For reference, the initial and final bottom profiles, including the MP release locations, are given in the top row of Fig. 4. Test series without vegetation (Fig. 4, column 1) indicate the direction of particle movement without influence of vegetation, which is illustrated with an arrow. The tests indicate that the particle group with the lowest tested particle Dean number tends to migrate offshore, while all other particle groups tend to migrate primarily onshore. This observation seems reasonable. The particles with the low particle Dean number have relatively low mobility and low transport rates. Due to stochastic variations, any particles reaching a point offshore of the bar crest are dominated by gravitational forces. They are thus unable to be transported back onshore up the slope, which explains why a large number of them accumulated at the offshore toe (similar accumulation at the offshore toe was observed in the experiments of Guler et al. (2022)). The MP Dean numbers are lower than the sand Dean number ($\Omega_s = 3.4$). The MP in other words act similar to coarse grained sediments. Generally, there is natural grain sorting with a coarsening towards the beach (Edwards, 2001). This was also found by Mitzuani et al. (2003), who stated that coarse grains had a lower tendency to go in suspension and become transported offshore by the undertow. Coarse grain sands (and hence MP in the present study) will therefore primarily be transported near the bed, whereas particles with a higher particle Dean number can be temporarily suspended e.g. by the breaking waves and, in the case of plunging breakers, be transported onshore into shallower water due to a phase coupling between onshore directed flow and turbulence (Guler et al., 2022). This process is also similar to what has been observed in the case of sediments (Christensen et al., 2019; Aagaard et al., 2021). Due to the stochastic nature of irregular waves a small number of particles behave differently, and some particles are found dispersed along the flume. The release point of the particles in the present tests with vegetation was selected accordingly, to ensure particle migration through the installed canopy.

The tested non-buoyant MP were transported by the wave-induced surf zone flows close to the bottom sand layer. The flow characteristics and transport mechanisms of MP over a barred beach profile without vegetation are described by Guler et al. (2022). They found a strong correlation between the particle Dean number and the particle mobility. Additionally, they identified that plunger-type breaking waves in the vicinity of the breaker play an important role for the on- and offshore transport of MP. The dimension of the sand ripples is oversized in the present study (as in all down-scaled hydraulic model tests; such features may even be absent in field conditions) (O'Donoghue et al., 2006). This might lead to an underestimation of the general mobility of particles

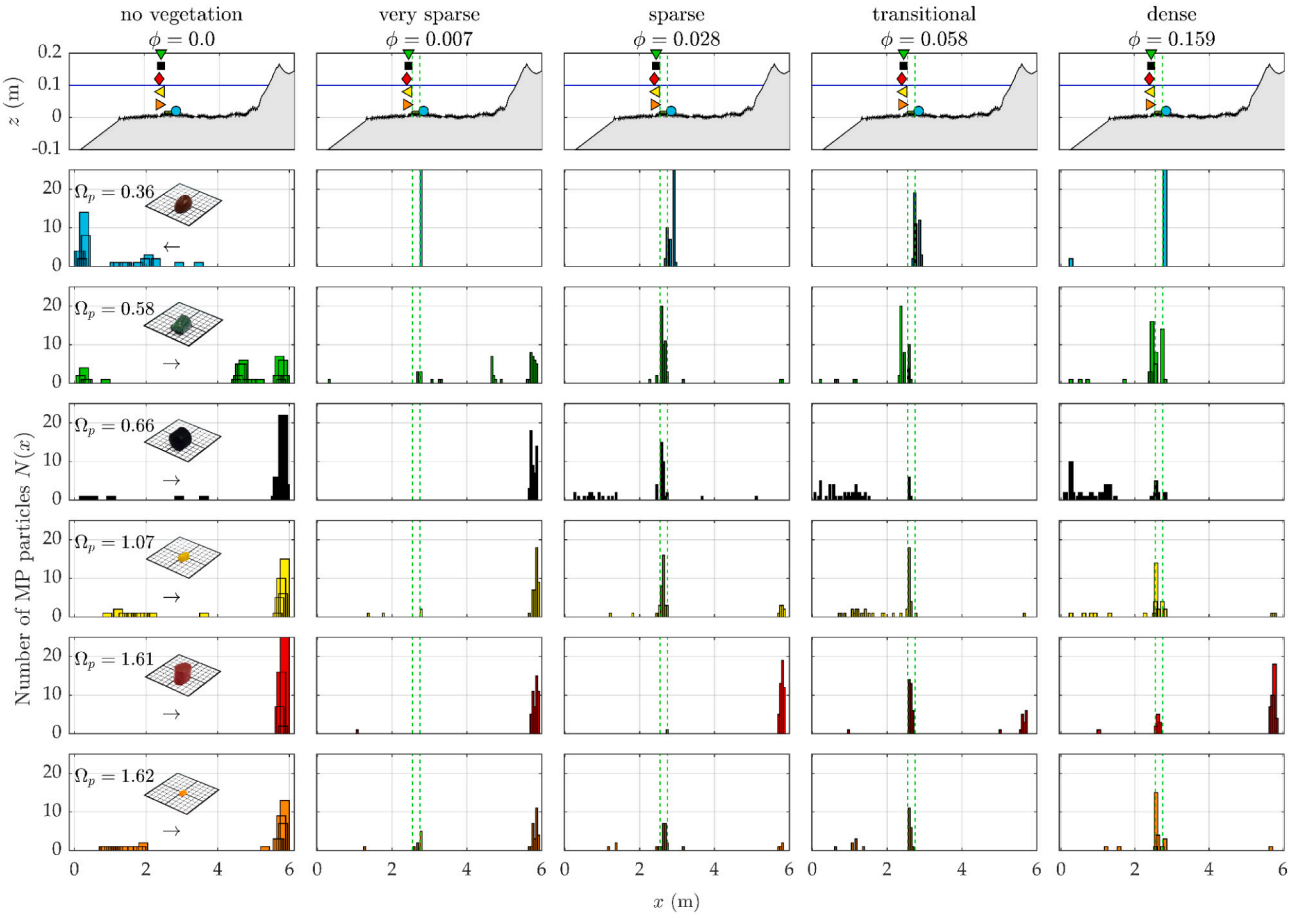

Fig. 4. Cross-shore distribution of the MP sampled at the end of each test run (number of buried and non-buried particles N at flume coordinate x) for no vegetation (1st column), very sparse canopies (2nd column) sparse canopies (3rd column), transitional canopies (4th column) and dense canopies (5th column). An image of each particle is given over millimeter scale in the first column. The location of the canopy is highlighted by the green dashed lines. Initial and final bottom profiles including the MP release locations are given in the top row. The cross-shore distribution of particles in ascending order of the particle Dean numbers (Ω_p) in the following rows. The MP migration direction without vegetation is indicated by arrows in the 1st column.

with low particle Dean number migrating in traction mode.

Independent of the canopy density, it is observed that the migration speed increases with particle Dean number, which makes physical sense, as these particles are more mobile (lower settling velocity). First, particles with $\Omega_p > 1.6$ generally reach their final accumulation hotspot after 10 min, while the transport of particles with $\Omega_p < 1.6$ took several hours. This observation is important, as this indicates that not all microplastic particles will reach their terminal positions during a storm. It is found that very sparse canopies are not able to sufficiently alter the flow regime to trap MP with particle Dean numbers $\Omega_p \leq 0.58$, and accumulation hotspots comparable to the unvegetated condition are found (Fig. 4, column 2). The wave energy throughout the vegetation height h_v is nonetheless sufficient to transport particles through the canopy (compare Fig. 2 and Fig. 3). Only particles with the lowest tested particle Dean number $\Omega_p = 0.36$ (i.e. less mobile particles having the largest settling velocity) are too inert and cease their migration through the lowest tested canopy density. With increasing canopy density most particle groups are trapped within the vegetated area (quantification follows in Fig. 5). Two considerable exceptions are to be mentioned. First, the majority of particles with $\Omega_p = 0.66$ reversed their migration direction in the presence of a vegetation canopy (for $\phi > 0.007$). It is assumed, that these particles migrate in saltation (bouncing) close to the bottom. As their onshore path is increasingly blocked by increasing vegetation density, they instead experience a net offshore migration, likely driven by the undertow and induced skewness in their transport behavior (asymmetric transport in positive and negative directions). Cases having the highest canopy density ultimately led to many particles accumulating at the offshore toe of the breaker bar, there likely driven by gravity, as similarly explained above for the case with $\Omega_p = 0.36$. Second, particles with $\Omega_p = 1.61$ were not trapped by the sparse vegetation, but were mostly trapped by the transitional vegetation, and somewhat trapped by the dense vegetation. As previously mentioned, it was observed that these particles were easily suspended by individual waves, due to their comparably low weight and hence settling velocity (Kerpen et al., 2023). Hence, the wave energy in the sparse canopy is nonetheless sufficient to transport these particles through the vegetation. In the transitional canopy, the particles are trapped in-between the individual plants. For the dense canopy it is observed that the diameter of these particles ($D_{N,p} = 2.8$ mm) is so large that the particles do not penetrate through the upper layer of the vegetation $\left(D_{N,p}/\left(S_{v,C} - d_{v,max}\right) > 1\right)$ and instead momentarily rest on top of the canopy. Subsequent waves may then re-suspend these particles and transport them over the canopy. In principle, the tested particles with $\Omega_p = 1.62$ follow the same transport mechanism. However, they have a smaller diameter $\left(D_{N,p} = 1.08\ \text{mm}\right)$. Accordingly, they do not rest on top of the dense canopy during transport and penetrate deeper into canopy regions with less wave energy before becoming trapped. Hence, the distance between individual shoots relative to the particle diameter $D_{N,p}/\left(\Delta S_{v,L}^2 + \Delta S_{v,C}^2\right)^{0.5}$ seems to play an important role for the retention of MP in canopies. This is the opposite of observations made in other studies (Gallitelli et al., 2023), which generally indicate an increase in the capture of plastic particles with increasing canopy density. The reasons for these differences could be that (i) their test series may not have been conducted for sufficient time (1 min test duration after the settling of the steady condition) and thus the entrapment is overestimated, (ii) they tested a larger particle size (5 mm $\leq D_{N,p} \leq$ 25 mm) or (iii) the particle penetration possibility ($D_{N,p} < \Delta S_{v,L}$) has not been taken into account so far as they studied different plant species (*Myriophyllum spicatum* and *Potamogeton crispus*). The particles not penetrating through the upper layer might be a scale effect, as the microplastic particles are not scaled. In field scales with a similar canopy density it would seem that a particle with $D_{N,p} = 2.8$ mm would likely be able to penetrate the upper layer. However, this observation might still be relevant for the fate of macro plastics (e.g. bottles or bags).

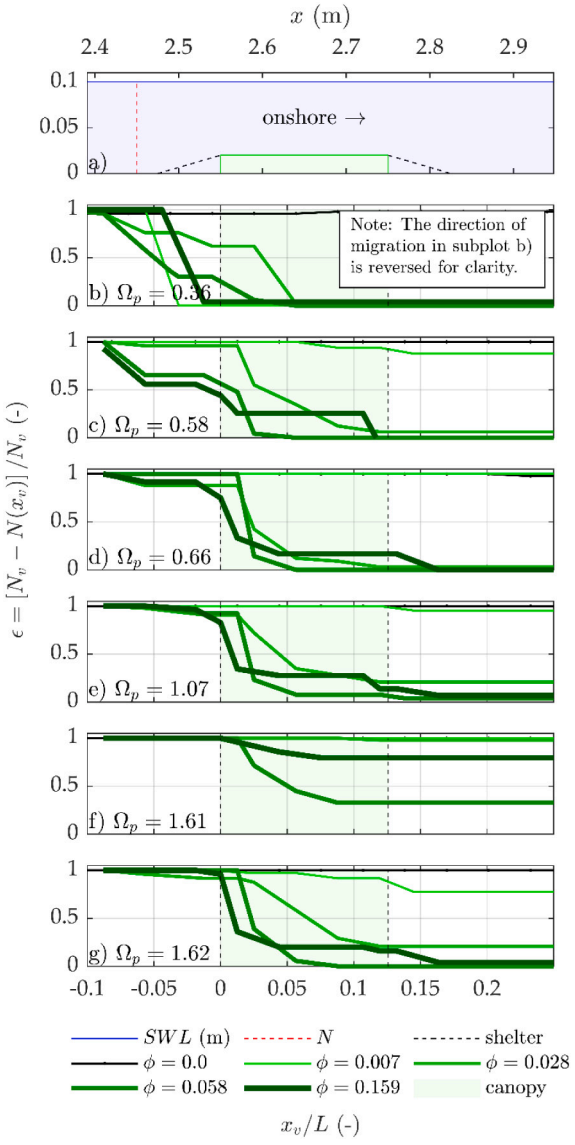

Fig. 5. (a) Geometry of the canopy (shaded green area) in the flume, MP input position (dashed red line) and shelter regions of lower wave energy in front of and behind the canopy (dashed black line). (b-g) Particle retention (number of buried and non-buried particles which deposit until location x_v ($N(x_v)$) relative to the total number of particles migrating through the canopy ($N_v = N - N_{\text{offshore}}$), solid green lines) for increasing penetration depth into the canopy ($x_v > 0$) normalized by the wave length L for varying canopy densities ($0 \leq \phi \leq 0.159$).

The present study shows that particles with high particle Dean number cross dense canopies more easily, provided that the canopy width is short ($B_v/L = 0.125$). It is assumed that the number of trapped particles increases with increasing canopy length. This assumption is justified by the continuous energy dissipation along the canopy (Eq. (A.4)), which further reduces the energy required for transport (Eq. (A.8)). If the transport energy becomes too low, these particles also sink into the canopy. For example, Gallitelli et al. (2023) found that higher plant density leads to higher entrapment of plastics by plants. The plant structure is a key factor in entrapping plastics. The present study shows that the particle retention of non-buoyant MP reduces with increasing flow velocity, decreasing shoot density and decreasing particle density in breaking-wave induced flows. MP having high density were trapped in wake regions close to the canopy. To date, these findings were only investigated for marine vegetated canopies under steady flow velocities

(2—30 cm/s) (de los Santos et al., 2021).

It was observed, that the canopy with the largest shoot density represented a kind of quasi-solid object for particles with larger diameter. This is an extremal boundary for the transport process. In consequence, particles did not migrate through the canopy, but rather over the canopy. During this process most of the particles lay on top of the canopy while they migrated onshore.

More inert particles ($\Omega_p = 0.36$) were (with stochastic exceptions) not able to migrate through any of the canopies. The reduced flow conditions close to the sediment bed directly behind the canopy shelter the heavy MP from further motion. It has also been observed by de Los Santos et al. (2021) that MP with higher density (thus, larger settling velocity and therefore a lower particle Dean number) tend to be trapped in regions with lower flow energy.

Having highlighted the global migration characteristics of MP in the tested vegetation canopies, focus will now be given to the quantification of the particle trapping within the canopies themselves. Fig. 5a provides the geometrical layout of the test section and the location where the MP are released. Shelter areas located off- and onshore of the canopy with prevailing reduced flow velocities are highlighted by a dashed black line. The quantitative retention of MP with increasing particle Dean number in the vegetation canopy is given in Fig. 5 (b-g). The migration direction in subfigure b) is displayed as reversed for clarity, as the particles with the lowest Dean number actually migrate in the offshore direction. It was decided to consider only those particles that actually moved through the vegetation during the experiment, in order to differentiate from those distributed along the channel against the main direction of migration (partly caused by stochastic outliers). Hence, the number of buried and non-buried particles counted at the location x_v ($N(x_v)$) at the end of a test ($t = 10$ h) is presented relative to the number of particles that migrated through the vegetation $N_v = N - N_{\text{offshore}}$. N represents the number of MP released at the beginning of the test at the location $x_{\text{start}} = 2.45$ m (and $t = 0$ h) and N_{offshore} the number of particles which changed migration direction towards offshore (vice versa for the particles with $\Omega_p = 0.36$) because of the presence of vegetation (compare Fig. 4). The particle transmission through a canopy is described by the particle transmission coefficient

$$\epsilon(x_v) = \frac{N_v - N(x_v)}{N_v}\begin{matrix}\rightarrow 0\text{:full retention in vegetation}\\ \rightarrow 1\text{:no retention in vegetation}\end{matrix} \tag{3}$$

which tends to zero when all particles are trapped in the canopy and tends to 1 when no particles are trapped by the canopy.

An increased percentage of particles were able to migrate through all tested canopies with increasing particle Dean number. With the exception of two outliers for the densest canopy (potentially caused by air bubbles adhering to the particles), particles having the lowest Dean number (particle 'L') were not able to migrate through any of the tested vegetation patches. On the other hand, at least approximately 50 % of all particles with one of the highest tested Dean number (particle 'G', $\Omega_p = 1.61$) were able to migrate through (or over) the tested vegetation. With some exceptions, the cause of which will be explained later, particles get caught a shorter migration distance into the canopy, and more often, in vegetation of higher density. It can also be seen, that particles with lower Dean number tend to deposit more readily in the wake regions close, before and behind the canopy. The promotion of sediment settling and resuspension reduction of particles in the wake regions behind a canopy is formerly documented (Villanueva et al., 2022, 2023). Likewise, e.g. the MP pollution in subtropical mangrove forests increases with increasing pneumatophore density (Duan et al., 2021). In their survey, an increased abundance of MP in samples collected at a mangrove forest fringe, compared to the mudflat or the forest interior, is documented. Hence, the canopy fringe provides a sieve-like filtering effect (see Fig. 4 and Fig. 5).

With respect to the statistical robustness of the findings, it has to be noted that the tests were repeated only once. On the other hand, the results are based on a high number of individual waves (>40,000 waves per test, Table 1) and each of these waves has the potential to transport the particles. For this reason, the observations on MP transport in vegetation are reliable.

4.4. Cross-shore particle migration ability

The particle transmission ϵ shall be described as a function of the properties of the MP ($\omega_{sp}; D_{N,p}$), the canopy density ϕ, the penetration depth into the canopy x_v and the local hydraulic loads u_b in the form:

$$\epsilon_{pred}(x_v) = f\left\{\phi; Fr_p = \frac{\omega_{sp}}{\sqrt{gD_{Np}}};\ \frac{\phi x_v}{A_p}\right\} \tag{4}$$

where $A_p = u_b T_p/(2\pi)$ is the maximum horizontal wave orbital excursion. The measured particle transmission ϵ (Eq. (3)) is expressed by the cumulative number of buried and non-buried particles N deposited at a location inside the canopy (x_v) relative to the number of particles that migrated into or through the canopy N_v.

First, the dependency of the transmission coefficient from the canopy density ϕ (Eq. (2)) is derived (Fig. 6a). For very sparse canopies ($\phi = 0.007$), the particle retention is low and ϵ tends to 1. For sparse ($\phi = 0.028$) and transitional ($\phi = 0.058$) canopies, the particle retention increases. Then, the particle retention decreases again with further increase of the canopy density ($\phi = 0.159$). This is plausible as particles cannot accumulate inside a theoretical rigid structure. It is observed that a dense canopy acts rather like a solid object, especially for large particles with a high particle Dean number. A higher particle Dean number expresses a higher resistance to the flow which allows for easier transport of these particles. MP with lower particle Dean numbers are not able to penetrate inside a canopy and hide in the fringe regions with reduced flow velocities in front of the canopy (compare Fig. 4 and Fig. 5). Therefore, it is plausible, that for $\phi = 1$ the particle transmission is $\epsilon < 1$. This influence of the canopy density on the particle transmission is described by the canopy density function:

$$f(\phi) = max\begin{cases} 1 - (33\phi)^2 \\ \sqrt{\phi} - 0.15 \end{cases} \tag{5}$$

Now, the influence of the particle properties on the particle transmission is analyzed. Small particle diameters ($D_{N,p} < 1$ mm) influence the particle drag disproportionately (Miedema, 2013). This influence is observed in the data (Fig. 6b) and can be expressed by the particle Froude number

$$Fr_p = \frac{\omega_{sp}}{\sqrt{gD_{N,p}}} \tag{6}$$

which relates the particle settling velocity with the particle diameter. Fig. 6b) reveals that the particle transmission, corrected against the influence of the canopy density $\epsilon/f(\phi)$, increases for particle Froude numbers $Fr_p < 0.4$ and tends to 1 for $Fr_p > 0.4$. The trend is described by the particle function

$$f(Fr_p) = 1 + (3.4Fr_p)^{-5} \tag{7}$$

The influence of the cross shore canopy dimension on the particle transmission is considered by relating the canopy density ϕ and particle penetration distance x_v relative to the maximum horizontal bottom flow amplitude $A_p = u_b T_p/(2\pi)$ to the relative particle transmission $\epsilon/(f(\phi)\cdot f(Fr_p))$ (Fig. 6c). The correlation is expressed with the canopy length function

$$f\left(\frac{x_v}{A_p}\right) = 1 + exp\left(-\frac{\phi x_v}{A_p}\right)^2 \tag{8}$$

The data reveal an increasing trend in the relative particle transmission $\epsilon/(f(\phi)\cdot f(Fr_p))$ with decreasing canopy penetration depth x_v of

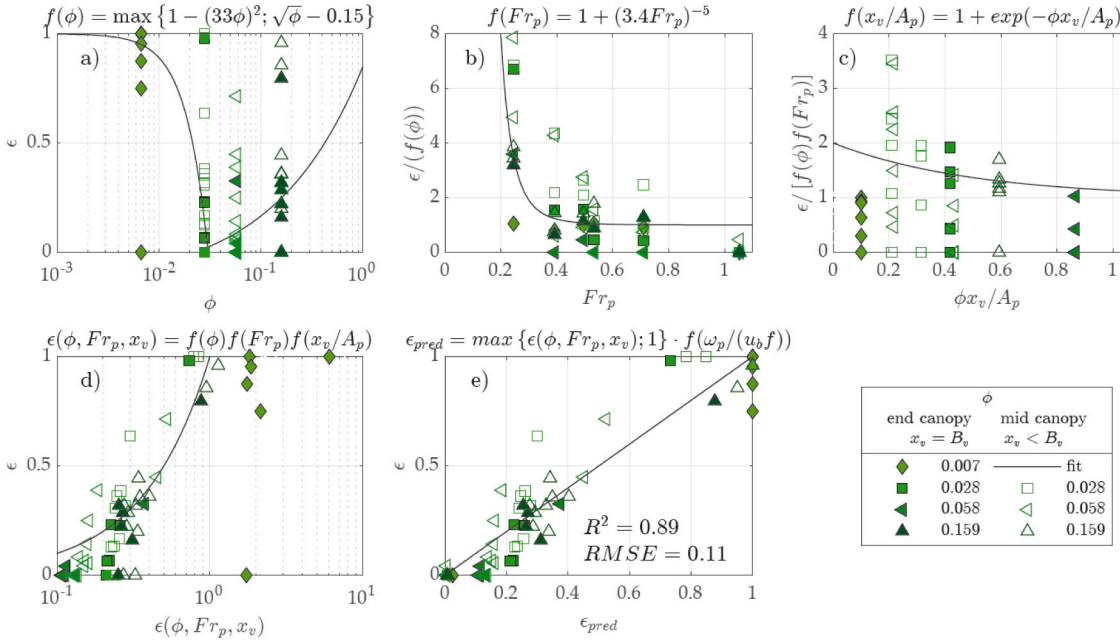

Fig. 6. Influence of a) the canopy density ϕ, b) the particle Froude number Fr_p and c) the relative canopy length $(\phi x_v/A_p)$ on the particle transmission ϵ through vegetation canopies with varying density ϕ. The correlation between the predicted (ϵ_{pred}) and measured (ϵ) particle transmission is given in d) without and in e) with a special consideration for very sparse canopies and more inert particles. The black solid line provides the best fit with a goodness of fit of $R^2 = 0.89$ with a root-mean-squared error of $RMSE = 0.11$.

the particles. But, with decreasing x_v, also the scatter increases caused by the quantification of N_{x_v} over a shorter distance. Eq. (8) overestimates the particle transmission for very sparse canopies ($\phi \leq 0.007$) which will be addressed in the following.

Fig. 6d) provides the correlation of the measured (ϵ) and the predicted particle transmission from Eq. (5), Eq. (7) and Eq. (8):

$$\epsilon\left(\phi, Fr_p, \frac{x_v}{A_p}\right) = f(\phi)\cdot f\left(Fr_p\right)\cdot f\left(\frac{x_v}{A_p}\right) \tag{9}$$

in a semi-logarithmic scale. In the present form, the prediction overestimates the particle retention for very sparse canopies ($\phi = 0.007$) and for particles with high settling velocities ($\omega_p > 0.17$, corresponds here to the data $\epsilon = 0$). The overestimation of the particle transmission for very sparse canopies is addressed in forthcoming Eq. (11) by maximizing ϵ_{pred} to 1. Additionally, the tests revealed that an initiation of particle motion did not occur when the settling velocity was too high in relation to the local flow velocity (no particle movement for $\omega_{sp} > 1.6u_b f$). Here, even the slightest change in the seabed caused the majority of particles to have no net movement, or even remain at the exact initial release location. From this observation, a threshold value for the initiation of the MP net motion into a canopy was derived in the form:

$$f\left(\frac{\omega_{sp}}{u_b f}\right) = \frac{1}{1+20\left\{1+tanh\left[500\left(\frac{\omega_{sp}}{u_b f}-1.6\right)\right]\right\}} \tag{10}$$

Following the approach of Eq. (4) by combining Eq. (9) and Eq. (10), the predicted particle transmisson through submerged vegetation canopies is finally expressed by:

$$\epsilon_{pred} = max\left\{\begin{matrix}\epsilon\left(\phi, Fr_p, \frac{x_v}{A_p}\right)\\ 1\end{matrix}\right\}\cdot f\left(\frac{\omega_{sp}}{u_b f}\right) \tag{11}$$

When ϵ_{pred} tends towards zero the resistance is high and particles are hindered to migrate through the canopy. For increasing ϵ_{pred} the particle mobility increases, whereas the canopy resistance decreases, and particle migration through the canopy becomes more likely.

The correlation between the predicted (ϵ_{pred}) and measured (ϵ) particle transmission in the tested canopies is given in Fig. 6e). The correlation is stronger for the data points for which the transmission was considered throughout the full canopy ($N_{x_v=B_v}$, filled symbols). When the particle retention is analyzed only up to a partial length of the canopy ($N_{x_v<B_v}$, blank symbols), thereby simulating data for a shorter canopy, the scattering increases. The outlier data (sparse canopy layout $\phi = 0.028$, square symbol, $\Omega_p = 1.61$) show a measured particle transmission of about $\epsilon = 1$ and a predicted particle transmission of about $\epsilon_{pred} = 0.8$. A cause for this deviation cannot be specified at present. The uncertainties from Eq. (11) are expressed by a goodness of fit of $R^2 = 0.89$ and a root mean squared error of 0.11. The application of Eq. (11) is limited to $0.007 \leq \phi \leq 0.159$ and $\Omega_p \geq 0.58$.

Previously determined wave and flow conditions interacting with marine vegetation canopies specified both the cross-shore distribution and migration ability of MP. Governing drivers in a laboratory setting have been revealed and clearly demonstrate the capacity and function of marine vegetated canopies to filter, block and trap MP pollutants. Other studies have disclosed similar behavior and performances, but until now, have only partly identified accumulation hotspots and drivers of transport and retention potential, which mimics a novel perspective on ecosystem service of subtidal coastal vegetation.

Eq. (11) will mostly be valid for vegetation patches on profiles with similar sand Dean numbers, waves coming perpendicular to the coast and vegetation patches placed within the surf zone. However, the qualitative description (not the direct bounds in the predictive equation) is more widely applicable.

4.5. Description of observed transport mechanisms

Fig. 7 summarizes the measured flow conditions (described in Section 4.2) of the present study and sets them qualitatively in the context of flows across and around vegetation canopies. On the left, an idealized undisturbed logarithmic velocity profile is shown in blue. Corresponding streamlines are given in grey. The streamlines shown correspond to a

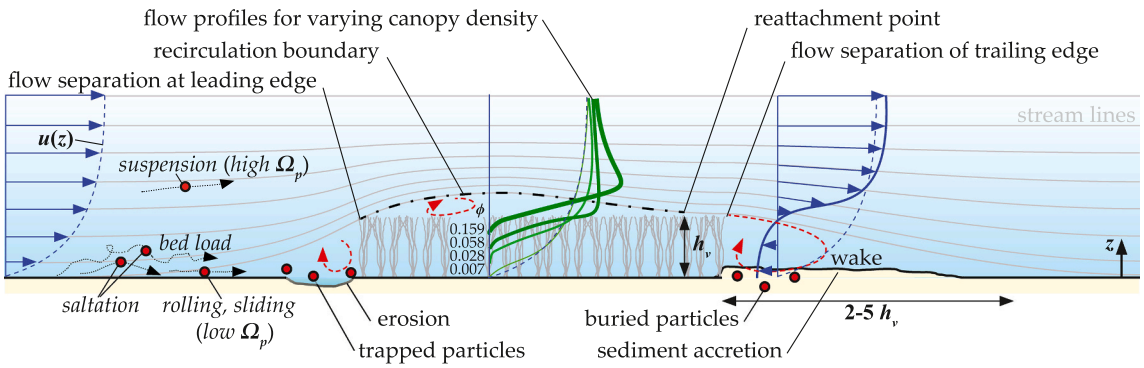

Fig. 7. Qualitative streamlines around the vegetation canopy with principle flow profiles for varying canopy densities. Wake region on the down-stream side of the canopy with principle recirculation flow profile (inspired by Cassiani et al. (2008)) which causes sediment accretion.

relatively impermeable canopy. As the canopy density decreases, the intensity of all the processes described in the following decrease in analogy. With flow propagation towards the canopy the flow is concentrated and accelerates above the canopy. At the leading edge of the canopy flow separation occurs, which indicates a clockwise vortex in the wake region. The downward flow in front of the canopy leads to local erosion effects. MP migrating in saltation and traction mode can be easily trapped in this flow-reduced region. In general, the ratio ω_{sp}/u_b is reduced in this region and the transportation mode of individual particles may change towards more of a near-bed transport behavior. Downstream of the leading canopy edge the streamlines form a recirculation boundary which ends further downstream at a reattachment point with the canopy. Below this recirculation boundary an area of undirected flow with strong three-dimensional-coherent turbulent structures (compare Fig. 2e), also known as the roughness sublayer (Ghisalberti and Nepf, 2008), is present. The retention time of transported MP is longer due to the unsteady flow with comparable low net velocity above the canopy in this area, which enables penetration into the canopy more likely. At the downstream side of the canopy the flow separates again at the canopy's tailing edge forming another wake region with a clockwise rotation vortex. The indicated flow profile reveals that this area promotes sedimentation, and MP in saltation and traction motion are trapped here and can be buried by sediments over time. Observations confirm the dimension of this downstream wake region in irregular breaking waves with 2–5 times the canopy height h_v (Fig. 5c) which was formerly quantified by Cassiani et al. (2008) for air-flows across forests. For steady currents, the dimension of the wake region behind a seagrass canopy is up to 5 times the canopy height (Villanueva et al., 2022). Particles that migrate predominantly in suspension should generally be less likely to have their migration hindered by vegetation, as these particles will follow the streamlines to evade the vegetation (Fig. 4, high particle Dean numbers).

5. Conclusions

By means of controlled hydraulic model (wave flume) tests with irregular breaking waves, the migration of MP with varying size and density through artificial, rigid and flexible vegetation canopies over a mobile sand bed has been studied. For the first time, migration ability of MP through vegetation has been quantified for breaking waves in the surf zone. It was found, that the MP migration ability depends on (i) the MP mobility itself, expressed by the particle Dean number Ω_p, (ii) the canopy characteristic length and density and (iii) the energy dissipation above the canopy, following an approach by Dalrymple et al. (1984), with a vegetation drag coefficient calculated by Wang et al. (2019). These boundary conditions were combined in an empirically derived correlation which also covers a special case for very dense vegetation. More inert MP with corresponding low particle Dean numbers tend to migrate closer to the sand bed and were more likely to be trapped in wake regions in front of and behind vegetation canopies, as well as in canopies of comparably low density. The dimension of the wake regions in front of and behind a submerged canopy in irregular breaking waves was in the range of 2—5 times the canopy height and therefore comparable to observations from steady flows. Heavy particles were buried below accreting sediments over time. MP with a settling velocity lower than the local flow velocity were suspended by the flow and could be transported more easily over short canopies, having dimensions smaller than the local wave length. Sparse canopies were too transparent to trap MP with particle Dean numbers $\Omega_p \leq 0.58$ and therefore can effectively be treated as unvegetated. For very dense canopies it was shown that particles with a diameter close to or larger than the distance of individual plants are less trapped. Previously only confirmed for uniform flows, the formation of a shear area above the canopy with increased flow acceleration for increasing canopy density was also identified herein for surf zone flow conditions. An increased retention of MP in vegetation with increasing shoot density, the MP specific density or the reduction of the flow velocity – also formerly only proven for stationary currents – can now likewise be confirmed for wave-driven surf zone flows.

Besides the widely acknowledged ecosystem services of submerged coastal vegetation, encompassing habitat provision, nutrient cycling and sediment stabilization (Duarte et al., 2013), it has been demonstrated that these marine canopies function as a native sink for MP, hindering their unimpeded dispersion in the water column. Thus, submerged vegetation in coastal regions concentrates the MP pollution in aquatic ecosystems, particularly in their fringe regions. On the one hand, this can be interpreted as positive for the pollution in the water column. On the other hand, this proves that a hotspot for biodiversity also becomes a hotspot for concentrated pollution. Based on this study it should be possible to better evaluate where to explore areas for MP accumulation in the vicinity of subtidal coastal vegetation. This allows technologies and measures to be developed for potential cleaning and removing MP, as it can now be determined where it is approximately located. Potential removal of MP from these areas would then be less costly, and the intervention in nature can hopefully be concentrated over smaller areas.

It would be of interest to test the applicability of the presented approach for canopies with dimensions wider than a wave length in future investigations, as it is assumed that these canopies could trap significantly more MP. Furthermore, an extension of the hydraulic boundary conditions would be interesting as the migration ability of the MP in the present study varied only in the particle properties (e.g. settling velocity) themselves, and not by a variation of the load scenario. As only the cross shore migration of MP has been studied it would be interesting to conduct tests in a 3D wave basin in order to quantify also the long shore transport.

CRediT authorship contribution statement

Nils B. Kerpen: Conceptualization, Formal analysis, Funding acquisition, Investigation, Methodology, Validation, Visualization, Writing – original draft, Writing – review & editing. **Bjarke Eltard Larsen:** Formal analysis, Funding acquisition, Methodology, Writing – original draft, Writing – review & editing. **Torsten Schlurmann:** Funding acquisition, Supervision, Writing – original draft, Writing – review & editing. **Maike Paul:** Writing – original draft, Writing – review & editing. **Hasan Gokhan Guler:** Writing – review & editing. **Koray Deniz Goral:** Writing – review & editing. **Stefan Carstensen:** Funding acquisition, Writing – review & editing. **Erik Damgaard Christensen:** Funding acquisition, Writing – review & editing. **David R. Fuhrman:** Funding acquisition, Methodology, Project administration, Supervision, Writing – review & editing.

Declaration of competing interest

David R. Fuhrman reports financial support was provided by Independent Research Fund Denmark. David R. Fuhrman reports a relationship with Independent Research Fund Denmark that includes: funding grants.

Data availability

Data will be available at the reserved DOI: https://doi.org/10.11583/DTU.22801799. A private link is provided in the manuscript, providing potential access for peer reviewers.

Acknowledgements

Parts of this research has been financially supported by the Independent Research Fund Denmark project MPCOAST MicroPlastic transport processes in the COASTal environment, grant no. 0136-00227B. The authors likewise acknowledge the support of Lisanne Georgi for assisting during the hydraulic model testing and Maximilian Behnke for 3D-printing the specimen and parts of the set-up. Alexander Schendel contributed with discussions about principle sediment transport mechanisms.

Appendix A. Analytical considerations

Geometric properties, as well as kinematic and dynamic processes, will are described for the study area. Sediment properties are excluded from the analytical consideration as the transport mechanism of MP over a quasi-steady beach profile is in the focus and significant hiding and exposure effects between sediment and MP were not observed. Hence, the following physical quantities for describing the local wave conditions, the fluid properties, the MP properties and the characteristics of the vegetation canopy are identified, based on the considerations provided in Section 2, to potentially describe the wave-driven transport of MP through a vegetation canopy:

$$\underbrace{H_{m0}(x), T_p(x), d(x)}_{\text{wave}}, \underbrace{\nu, \rho_f}_{\text{fluid}}, \underbrace{g}_{\text{kinematic, dynamic}}, \underbrace{d_v, b_v, h_v, \Delta S_{v,L}, \Delta S_{v,C}, B_v}_{\text{vegetation}}, \underbrace{D_{N,p}, \rho_p, \omega_{sp}}_{\text{microplastic}} \tag{A.1}$$

Here g is the acceleration of gravity and B_v the cross-shore width of the canopy.

Since the non-buoyant MP rest on the sediment bed at the beginning of an experiment, the near-bed flow velocity u_b is of interest. The magnitude of the near-bed flow velocity can be approximated as that at the bed based on linear wave theory:

$$u_{b,max} = \frac{H_{m0}\pi}{T_p} \frac{1}{\sinh(k_p d)} \tag{A.2}$$

considering local wave conditions. The Root Mean Square (RMS) flow velocity likewise corresponds approximately to:

$$\widetilde{u} = \frac{u_{b,max}}{\sqrt{2}} \tag{A.3}$$

The presence of a submerged vegetation canopy increases the bottom friction compared to a flat sand bed. Following Eq. (A.2), the near-bed flow velocity is directly dependent on the wave height. The influence of an increased bottom friction can thus be derived from the wave decay over the submerged vegetation. For a given cross-shore position x_v in the canopy (with $x_v = 0$ at the offshore fringe), the decay of the wave height $H(x_v = 0)$ is described by Dalrymple et al. (1984), so that the relation to a wave height $H(x_v)$ in or at the onshore-located end of a canopy (or the height of the transmitted wave $H_t = H(x_v = B_v)$) can be described by:

$$f = \frac{H_t}{H(x_v = 0)} = \frac{1}{1 + \alpha x_v} \tag{A.4}$$

The damping factor

$$\alpha = \frac{2C_{D,v}}{3\pi} \frac{\overline{d_v}}{\Delta S_{v,L}} \frac{H(x_v = 0)}{2\Delta S_{v,L}} \left(\sinh^3 k h_v + 3 \sinh k h_v\right) \left[\frac{4k}{3\sin\ kd\ (\sinh 2kd + 2kd)}\right] \tag{A.5}$$

(having inverse length units) accounts for the vegetation properties, namely the mean plant width $\overline{d_v} = \frac{1}{d_v^{-0.5} d_{v,max}^{-0.5}}$, the long-shore plant spacing $\Delta S_{v,L}$, the height of the vegetation h_v and the canopy drag coefficient, which is calculated according to Wang et al. (2019):

$$C_{D,v} = 0.819 + \frac{58.8}{\sqrt{\frac{\pi(1-\phi)}{4\phi Re_v}}} \tag{A.6}$$

The canopy density ϕ is calculated from Eq. (2), and the canopy Reynolds number

$$Re_v = \frac{u_{b,max}\overline{d_v}}{\nu} \tag{A.7}$$

is calculated with the maximum near-bed velocity $u_{b,max}$ from Eq. (A.2). The settling of MP having diameter $D_{N,p}$ and density ρ_p following the direction of gravity g in a fluid with a density ρ_f induces a drag force $F_{d,p}$. Goral et al. (2023) provide an approach to calculate the MP drag coefficient (hence settling velocity) based on particle and fluid properties. In the present tests, ω_{sp} has been experimentally measured in the same aperture and procedure as described in Goral et al. (2023).

Relating the wave-induced near-bed flow velocity above the sediment bed $u_{b,max}$ from Eq. (A.2) and the vegetation-induced energy dissipation due to increased bottom friction f from Eq. (A.4) with the particle settling velocity ω_{sp} gives the dimensionless expression

$$\frac{\omega_{sp}}{u_{b,max} \cdot f} \tag{A.8}$$

which finally takes into account all physical quantities listed in Eq. (A.1).

References

Aagaard, T., Brinkkemper, J., Christensen, D.F., Hughes, M.G., Ruessink, G., 2021. Surf zone turbulence and suspended sediment dynamics—A review. Journal of Marine Science and Engineering 9, 1300. https://doi.org/10.3390/jmse9111300.

Ballent, A., Pando, S., Purser, A., Juliano, M.F., Thomsen, L., 2013. Modelled transport of benthic marine microplastic pollution in the Nazaré canyon. Biogeosciences 10, 7957–7970. https://doi.org/10.5194/bg-10-7957-2013.

Battisti, C., Fanelli, G., Gallitelli, L., Scalici, M., 2023. Dunal plants as sink for anthropogenic marine litter: the entrapping role of Salsola kali L. (1753) in a Mediterranean remote beach (Sardinia, Italy). Mar. Pollut. Bull. 192, 115033 https://doi.org/10.1016/j.marpolbul.2023.115033.

Ben-Haddad, M., Abelouah, M.R., Hajji, S., Rangel-Buitrago, N., Alla, A.A., 2023. The halophyte Cakile maritima Scop. 1772 as a trap of plastic litter on the Moroccan coast. Mar. Pollut. Bull. 187, 114574 https://doi.org/10.1016/j.marpolbul.2023.114574.

Bradley, K., Houser, C., 2009. Relative velocity of seagrass blades: implications for wave attenuation in low-energy environments. J. Geophys. Res. Earth 114. https://doi.org/10.1029/2007JF000951.

BSH, 2021. Sea state statistics of the tide gauge sylt for 2021. Available at: https://www2.bsh.de/aktdat/Seegang/statistik/2021/wes21/WES21.htm. Accessed July 26, 2023.

Cáceres, I., Alsina, J.M., 2012. A detailed, event-by-event analysis of suspended sediment concentration in the swash zone. Cont. Shelf Res. 41, 61–76. https://doi.org/10.1016/j.csr.2012.04.004.

Cassiani, M., Katul, G.G., Albertson, J.D., 2008. The effects of canopy leaf area index on airflow across Forest edges: large-eddy simulation and analytical results. Boundary-Layer Meteorol 126, 433–460. https://doi.org/10.1007/s10546-007-9242-1.

Christensen, D.F., Hughes, M.G., Aagaard, T., 2019. Wave period and grain size controls on short-wave suspended sediment transport under shoaling and breaking waves. J. Geophys. Res. Earth 124, 3124–3142. https://doi.org/10.1029/2019JF005168.

Chubarenko, I., Esiukova, E., Bagaev, A., Isachenko, I., Demchenko, N., Zobkov, M., et al., 2018. Chapter 6 - Behavior of Microplastics in Coastal Zones. In: Zeng, E.Y. (Ed.), Microplastic Contamination in Aquatic Environments. Elsevier, pp. 175–223. https://doi.org/10.1016/B978-0-12-813747-5.00006-0.

Contti Neto, N., Pomeroy, A., Lowe, R., Ghisalberti, M., 2022. Seagrass meadows reduce wind-wave driven sediment resuspension in a sheltered environment. Front. Mar. Sci. 8 https://doi.org/10.3389/fmars.2021.733542.

Cózar, A., Sanz-Martín, M., Martí, E., González-Gordillo, J.I., Ubeda, B., Gálvez, J.Á., et al., 2015. Plastic accumulation in the Mediterranean Sea. PLoS One 10, e0121762. https://doi.org/10.1371/journal.pone.0121762.

Dalrymple, R.A., Kirby, J.T., Hwang, P.A., 1984. Wave diffraction due to areas of energy dissipation. J. Waterw. Port Coast. Ocean Eng. 110, 67–79. https://doi.org/10.1061/(ASCE)0733-950X(1984)110:1(67).

Dean, R.G., Dalrymple, R.A., 1991. Water wave mechanics for engineers and scientists. World Scientific. https://doi.org/10.1142/1232. Available at. Accessed December 21, 2020.

Defina, A., Bixio, A.C., 2005. Mean flow and turbulence in vegetated open channel flow. Water Resour. Res. 41 https://doi.org/10.1029/2004WR003475.

Deudero, S., Alomar, C., 2015. Mediterranean marine biodiversity under threat: reviewing influence of marine litter on species. Mar. Pollut. Bull. 98, 58–68. https://doi.org/10.1016/j.marpolbul.2015.07.012.

Dietrich, W.E., 1982. Settling velocity of natural particles. Water Resour. Res. 18, 1615–1626. https://doi.org/10.1029/WR018i006p01615.

Dolch, T., Buschbaum, C., Reise, K., 2013. Persisting intertidal seagrass beds in the northern Wadden Sea since the 1930s. J. Sea Res. 82, 134–141. https://doi.org/10.1016/j.seares.2012.04.007.

Duan, J., Han, J., Cheung, S.G., Chong, R.K.Y., Lo, C.-M., Lee, F.W.-F., et al., 2021. How mangrove plants affect microplastic distribution in sediments of coastal wetlands: case study in Shenzhen Bay, South China. Sci. Total Environ. 767, 144695 https://doi.org/10.1016/j.scitotenv.2020.144695.

Duarte, C.M., Losada, I.J., Hendriks, I.E., Mazarrasa, I., Marbà, N., 2013. The role of coastal plant communities for climate change mitigation and adaptation. Nat. Clim. Chang. 3, 961–968. https://doi.org/10.1038/nclimate1970.

Edwards, A.C., 2001. Grain size and sorting in modern beach sands. J. Coast. Res. 17, 38–52.

Eklöf, J.S., Donadi, S., van der Heide, T., van der Zee, E.M., Eriksson, B.K., 2015. Effects of antagonistic ecosystem engineers on macrofauna communities in a patchy, intertidal mudflat landscape. J. Sea Res. 97, 56–65. https://doi.org/10.1016/j.seares.2014.12.003.

Everaert, G., Van Cauwenberghe, L., De Rijcke, M., Koelmans, A.A., Mees, J., Vandegehuchte, M., et al., 2018. Risk assessment of microplastics in the ocean: modelling approach and first conclusions. Environ. Pollut. 242, 1930–1938. https://doi.org/10.1016/j.envpol.2018.07.069.

Forsberg, P.L., Sous, D., Stocchino, A., Chemin, R., 2020. Behaviour of plastic litter in nearshore waters: first insights from wind and wave laboratory experiments. Mar. Pollut. Bull. 153, 111023 https://doi.org/10.1016/j.marpolbul.2020.111023.

Galgani, F., Hanke, G., Werner, S., Oosterbaan, L., Nilsson, P., Fleet, D., et al., 2013. Guidance on Monitoring of Marine Litter in European Seas. Publications Office of the European Union, Lucembourg. https://doi.org/10.2788/99475. Available at:

Gallitelli, L., Di Lollo, G., Adduce, C., Maggi, M.R., Trombetta, B., Scalici, M., 2023. Aquatic plants entrap different size of plastics in indoor flume experiments. Sci. Total Environ. 863, 161051 https://doi.org/10.1016/j.scitotenv.2022.161051.

Gerritse, J., Leslie, H.A., de Tender, C.A., Devriese, L.I., Vethaak, A.D., 2020. Fragmentation of plastic objects in a laboratory seawater microcosm. Sci. Rep. 10, 10945. https://doi.org/10.1038/s41598-020-67927-1.

Ghisalberti, M., Nepf, H., 2008. Shallow flows over a permeable medium: the hydrodynamics of submerged aquatic canopies. Transp. Porous Media 78, 309–326. https://doi.org/10.1007/s11242-008-9305-x.

Gijón Mancheño, A., Jansen, W., Winterwerp, J.C., Uijttewaal, W.S.J., 2021. Predictive model of bulk drag coefficient for a nature-based structure exposed to currents. Sci. Rep. 11, 3517. https://doi.org/10.1038/s41598-021-83035-0.

Goral, K.D., Guler, H.G., Eltard Larsen, B., Carstensen, S., Christensen, E.D., Kerpen, N.B., et al., 2023. Settling velocity of microplastic particles having regular and irregular shapes. Environ. Res. 115783 https://doi.org/10.1016/j.envres.2023.115783.

Guler, H.G., Larsen, B.E., Quintana, O., Goral, K.D., Carstensen, S., Christensen, E.D., et al., 2022. Experimental study of non-buoyant microplastic transport beneath breaking irregular waves on a live sediment bed. Mar. Pollut. Bull. 181, 113902 https://doi.org/10.1016/j.marpolbul.2022.113902.

Harris, P.T., 2020. The fate of microplastic in marine sedimentary environments: A review and synthesis. Mar. Pollut. Bull. 158, 111398 https://doi.org/10.1016/j.marpolbul.2020.111398.

Hasselmann, K., 1973. Measurements of Wind-Wave Growth and Swell Decay during the Joint North Sea Wave Project (JONSWAP). Dt. Hydrograph. Inst, Hamburg.

Huang, Y., Xiao, X., Xu, C., Perianen, Y.D., Hu, J., Holmer, M., 2020. Seagrass beds acting as a trap of microplastics - emerging hotspot in the coastal region? Environ. Pollut. 257, 113450 https://doi.org/10.1016/j.envpol.2019.113450.

Inman, D.L., 1949. Sorting of sediments in the light of fluid mechanics. J. Sediment. Res. 19, 51–70. https://doi.org/10.1306/D426934B-2B26-11D7-8648000102C1865D.

Jacobsen, N.G., McFall, B.C., 2022. Wave-averaged properties for non-breaking waves in a canopy: viscous boundary layer and vertical shear stress distribution. Coast. Eng. 174, 104117 https://doi.org/10.1016/j.coastaleng.2022.104117.

van Katwijk, M.M., Bos, A.R., Hermus, D.C.R., Suykerbuyk, W., 2010. Sediment modification by seagrass beds: Muddification and sandification induced by plant cover and environmental conditions. Estuar. Coast. Shelf Sci. 89, 175–181. https://doi.org/10.1016/j.ecss.2010.06.008.

Kerpen, N.B., Larsen, B.E., Schlurmann, T., Paul, M., Guler, H.G., Goral, K.D., Carstensen, S., Christensen, E.D., Fuhrman, D.R., 2023. Dataset for "Microplastic retention in marine vegetation canopies under breaking irregular waves. Technical University of Denmark. https://doi.org/10.11583/DTU.22801799.

Kerpen, N.B., Schlurmann, T., Schendel, A., Gundlach, J., Marquard, D., Hüpgen, M., 2020. Wave-induced distribution of microplastic in the surf zone. Front. Mar. Sci. 7, 979. https://doi.org/10.3389/fmars.2020.590565.

Krause-Jensen, D., Middelboe, A.L., Sand-Jensen, K., Christensen, P.B., 2000. Eelgrass, Zostera marina, growth along depth gradients: upper boundaries of the variation as a powerful predictive tool. Oikos 91, 233–244.

Larsen, B.E., Al-Obaidi, M.A.A., Guler, H.G., Carstensen, S., Goral, K.D., Christensen, E.D., et al., 2023a. Experimental investigation on the nearshore transport of buoyant

microplastic particles. Mar. Pollut. Bull. 187, 114610 https://doi.org/10.1016/j.marpolbul.2023.114610.
Larsen, B.E., van der A, D.A., Carstensen, R., Carstensen, S., Fuhrman, D.R., 2023b. Experimental investigation on the effects of shoreface nourishment placement and timing on long-term cross-shore profile development. Coast. Eng. 180, 104258 https://doi.org/10.1016/j.coastaleng.2022.104258.
Lawson, S.E., Wiberg, P.L., McGlathery, K.J., Fugate, D.C., 2007. Wind-driven sediment suspension controls light availability in a shallow coastal lagoon. Estuaries and Coasts: J ERF 30, 102–112. https://doi.org/10.1007/BF02782971.
Li, Q., Su, L., Ma, C., Feng, Z., Shi, H., 2022. Plastic debris in coastal macroalgae. Environ. Res. 205, 112464 https://doi.org/10.1016/j.envres.2021.112464.
de los Santos, C.B., Onoda, Y., Vergara, J.J., Pérez-Lloréns, J.L., Bouma, T.J., Nafie, Y.A. L., et al., 2016. A comprehensive analysis of mechanical and morphological traits in temperate and tropical seagrass species. Mar. Ecol. Prog. Ser. 551, 81–94. https://doi.org/10.3354/meps11717.
de los Santos, C.B., Krång, A.-S., Infantes, E., 2021. Microplastic retention by marine vegetated canopies: simulations with seagrass meadows in a hydraulic flume. Environ. Pollut. 269, 116050 https://doi.org/10.1016/j.envpol.2020.116050.
Maghsodian, Z., Sanati, A.M., Tahmasebi, S., Shahriari, M.H., Ramavandi, B., 2022. Study of microplastics pollution in sediments and organisms in mangrove forests: A review. Environ. Res. 208, 112725 https://doi.org/10.1016/j.envres.2022.112725.
Miedema, S.A., 2013. An overview of theories describing head losses in slurry transport: A tribute to some of the early researchers. In: American Society of Mechanical Engineers Digital Collection. https://doi.org/10.1115/OMAE2013-10521.
Mitzuani, N., Ma, H.-H., Eguchi, S., 2003. An experimental study on the beach profile change and grading process of beach material. In: Proc. 13'th Int. Offshore and Polar Eng. Conf. (Honolulu, Hawaii, USA), pp. 864–869.
Nepf, H., Ghisalberti, M., White, B., Murphy, E., 2007. Retention time and dispersion associated with submerged aquatic canopies. Water Resour. Res. 43 https://doi.org/10.1029/2006WR005362.
Nepf, H.M., 2012. Flow and transport in regions with aquatic vegetation. Annu. Rev. Fluid Mech. 44, 123–142. https://doi.org/10.1146/annurev-fluid-120710-101048.
Nepf, H.M., Vivoni, E.R., 2000. Flow structure in depth-limited, vegetated flow. J. Geophys. Res. Oceans 105, 28547–28557. https://doi.org/10.1029/2000JC900145.
Newell, R.I.E., Koch, E.W., 2004. Modeling seagrass density and distribution in response to changes in turbidity stemming from bivalve filtration and seagrass sediment stabilization. Estuaries 27, 793–806. https://doi.org/10.1007/BF02912041.
Nielsen, P., 2009. Coastal and Estuarine Processes. World Scientific Publishing Company, Singapore.
Nordlund, L.M., Koch, E.W., Barbier, E.B., Creed, J.C., 2016. Seagrass ecosystem services and their variability across genera and geographical regions. PLoS One 11, e0163091. https://doi.org/10.1371/journal.pone.0163091.
Núñez, P., Romano, A., García-Alba, J., Besio, G., Medina, R., 2023. Wave-induced cross-shore distribution of different densities, shapes, and sizes of plastic debris in coastal environments: A laboratory experiment. Mar. Pollut. Bull. 187, 114561 https://doi.org/10.1016/j.marpolbul.2022.114561.
O'Donoghue, T., Doucette, J.S., van der Werf, J.J., Ribberink, J.S., 2006. The dimensions of sand ripples in full-scale oscillatory flows. Coast. Eng. 53, 997–1012. https://doi.org/10.1016/j.coastaleng.2006.06.008.
Ogbuagu, C.C., Kassem, H., Udiba, U.U., Stead, J.L., Cundy, A.B., 2022. Role of saltmarsh systems in estuarine trapping of microplastics. Sci. Rep. 12, 15546. https://doi.org/10.1038/s41598-022-18881-7.
Paul, M., Amos, C.L., 2011. Spatial and seasonal variation in wave attenuation over Zostera noltii. J. Geophys. Res. Oceans 116. https://doi.org/10.1029/2010JC006797.
Paul, M., de los Santos, C.B., 2019. Variation in flexural, morphological, and biochemical leaf properties of eelgrass (Zostera marina) along the European Atlantic climate regions. Mar. Biol. 166, 127. https://doi.org/10.1007/s00227-019-3577-2.
Pujol, D., Serra, T., Colomer, J., Casamitjana, X., 2013. Flow structure in canopy models dominated by progressive waves. J. Hydrol. 486, 281–292. https://doi.org/10.1016/j.jhydrol.2013.01.024.
Raupach, M.R., Finnigan, J.J., Brunei, Y., 1996. Coherent eddies and turbulence in vegetation canopies: the mixing-layer analogy. Boundary-Layer Meteorol 78, 351–382. https://doi.org/10.1007/BF00120941.
Sanchez-Vidal, A., Canals, M., de Haan, W.P., Romero, J., Veny, M., 2021. Seagrasses provide a novel ecosystem service by trapping marine plastics. Sci. Rep. 11, 254. https://doi.org/10.1038/s41598-020-79370-3.
Schubert, P.R., Hukriede, W., Karez, R., Reusch, T.B.H., 2015. Mapping and modeling eelgrass Zostera marina distribution in the western Baltic Sea. Mar. Ecol. Prog. Ser. 522, 79–95.
Scott, C.P., Cox, D.T., Maddux, T.B., Long, J.W., 2005. Large-scale laboratory observations of turbulence on a fixed barred beach. Meas. Sci. Technol. 16, 1903. https://doi.org/10.1088/0957-0233/16/10/004.
van Sebille, E., Aliani, S., Law, K.L., Maximenko, N., Alsina, J.M., Bagaev, A., et al., 2020a. The physical oceanography of the transport of floating marine debris. Environ. Res. Lett. 15, 023003 https://doi.org/10.1088/1748-9326/ab6d7d.
van Sebille, E., Aliani, S., Law, K.L., Maximenko, N., Alsina, J.M., Bagaev, A., et al., 2020b. The physical oceanography of the transport of floating marine debris. Environ. Res. Lett. 15, 023003 https://doi.org/10.1088/1748-9326/ab6d7d.
da Silva Paes, E., Gloaguen, T.V., dos Anjos da Conceição Silva, H., Duarte, T.S., da Conceição de Almeida, M., Costa, O.D.V., et al., 2022. Widespread microplastic pollution in mangrove soils of Todos os Santos Bay, northern Brazil. Environ. Res. 210, 112952 https://doi.org/10.1016/j.envres.2022.112952.
de Smit, J.C., Anton, A., Martin, C., Rossbach, S., Bouma, T.J., Duarte, C.M., 2021. Habitat-forming species trap microplastics into coastal sediment sinks. Sci. Total Environ. 772, 145520 https://doi.org/10.1016/j.scitotenv.2021.145520.
Song, Y.K., Hong, S.H., Jang, M., Han, G.M., Jung, S.W., Shim, W.J., 2017. Combined effects of UV exposure duration and mechanical abrasion on microplastic fragmentation by polymer type. Environ. Sci. Technol. 51, 4368–4376. https://doi.org/10.1021/acs.est.6b06155.
Soulsby, R., 1997. Dynamics of Marine Sands: A Manual for Practical Applications. Thomas Telford, London, UK.
Ting, F.C.K., Kirby, J.T., 1994. Observation of undertow and turbulence in a laboratory surf zone. Coast. Eng. 24, 51–80. https://doi.org/10.1016/0378-3839(94)90026-4.
Valero, D., Belay, B.S., Moreno-Rodenas, A., Kramer, M., Franca, M.J., 2022. The key role of surface tension in the transport and quantification of plastic pollution in rivers. Water Res. 226, 119078 https://doi.org/10.1016/j.watres.2022.119078.
Van der Zanden, J., Van der A, D.A., Hurther, D., Cáceres, I., O'Donoghue, T., Ribberink, J.S., 2016. Near-bed hydrodynamics and turbulence below a large-scale plunging breaking wave over a mobile barred bed profile. J. Geophys. Res. Oceans 121, 6482–6506. https://doi.org/10.1002/2016JC011909.
Van der Zanden, J., Van der A, D.A., Hurther, D., Cáceres, I., O'Donoghue, T., Hulscher, S.J.M.H., et al., 2017. Bedload and suspended load contributions to breaker bar morphodynamics. Coast. Eng. 129, 74–92. https://doi.org/10.1016/j.coastaleng.2017.09.005.
Van Rijn, L.C., 1993. Principles of Sediment Transport in Rivers, Estuaries and Coastal Seas. Aqua publications Amsterdam, Amsterdam.
Van Veelen, T.J., Fairchild, T.P., Reeve, D.E., Karunarathna, H., 2020. Experimental study on vegetation flexibility as control parameter for wave damping and velocity structure. Coast. Eng. 157, 103648 https://doi.org/10.1016/j.coastaleng.2020.103648.
Villanueva, R., Thom, M., Visscher, J., Paul, M., Schlurmann, T., 2022. Wake length of an artificial seagrass meadow: a study of shelter and its feasibility for restoration. Journal of Ecohydraulics 7, 77–91. https://doi.org/10.1080/24705357.2021.1938256.
Villanueva, R., Paul, M., Schlurmann, T., 2023. Wave dynamics alteration by discontinuous flexible mats of artificial seagrass can support seagrass restoration efforts. Sci. Rep. 13, 19418. https://doi.org/10.1038/s41598-023-46612-z.
Waldschläger, K., Schüttrumpf, H., 2019. Effects of particle properties on the settling and rise velocities of microplastics in freshwater under laboratory conditions. Environ. Sci. Technol. 53, 1958–1966. https://doi.org/10.1021/acs.est.8b06794.
Wang, W.-J., Huai, W.-X., Li, S., Wang, P., Wang, Y.-F., Zhang, J., 2019. Analytical solutions of velocity profile in flow through submerged vegetation with variable frontal width. J. Hydrol. 578, 124088 https://doi.org/10.1016/j.jhydrol.2019.124088.
Ward, L.G., Michael Kemp, W., Boynton, W.R., 1984. The influence of waves and seagrass communities on suspended particulates in an estuarine embayment. Mar. Geol. 59, 85–103. https://doi.org/10.1016/0025-3227(84)90089-6.
Wessel, C.C., Lockridge, G.R., Battiste, D., Cebrian, J., 2016. Abundance and characteristics of microplastics in beach sediments: insights into microplastic accumulation in northern Gulf of Mexico estuaries. Mar. Pollut. Bull. 109, 178–183. https://doi.org/10.1016/j.marpolbul.2016.06.002.
Yalin, M.S., 1977. Mechanics of Sediment Transport. Pergamon Press, Oxford.
Zhang, H., 2017. Transport of microplastics in coastal seas. Estuar. Coast. Shelf Sci. 199, 74–86. https://doi.org/10.1016/j.ecss.2017.09.032.